Journal of Materials Chemistry A

Accepted Manuscript

ROYAL SOCIETY OF CHEMISTRY

www.rsc.org/materialsA

Journal of Materials Chemistry A

ARTICLE

Silver-Copper Metallic Glass Electrocatalyst with High Activity and Stability Comparable to Pt/C for Zinc–Air Batteries

Received 00th January 20xx,
Accepted 00th January 20xx

DOI: 10.1039/x0xx00000x

www.rsc.org/

Xiaoqiang Wu,[a] Fuyi Chen,[a] Nan Zhang,[a] Adnan Qaseem[a] and Roy L. Johnston[b]*

Highly active electrocatalysts with good long term stability are vital for the commercialization of metal air batteries and alkaline fuel cells which involve the oxygen reduction reaction (ORR) at the cathode end. Herein, we developed a pulsed laser deposition (PLD) technique for the precise fabrication of silver-copper metallic glass(AgCu-MG) electrocatalysts. This PLD technique provides excellent control over the surface microtopography along with high flexibility for the deposition of different compositions of silver-copper metallic glass electrocatalysts onto nickel foam. Among all investigated Ag- based catalysts, AgCu-MG catalysts exhibits high electrocatalytic activity with the half potential of 0. 67V (vs. RHE) which can be in-situ enhanced by dealloying treatment in N_2 saturated 0.1 M KOH solution. In-situ dealloying of the AgCu-MG renders exceptional ORR catalytic activity with a half-potential of 0.78 V(vs.RHE) at 1600 rpm, which is comparable to commercial 0.81 V (vs.RHE) of Pt/C-20%. The AgCu-MG electrocatalyst showed excellent long-term stability in rechargeable zinc-air battery. After 1000 charge-discharge cycles at 20 mA cm^{-2}, the discharge voltage of battery was stable at 1.0V demonstrating the potential application of AgCu-MG as an alternative to Pt/C-20% in zinc-air battery and alkaline fuel cells.

Introduction

The commercialization of metal air battery systems such as zinc-air and lithium-air batteries requires to overcome challenges including high cost, low activity and stability.[1-3] Pt based nanoalloys are generally used as ORR catalyst but their high cost and scarce deposits within the earth crust provides the motivation to look for other alternatives.[4-7] Recently, a lot of attention has been focused on Ag based nanoalloys, which form an attractive catalyst system because of being roughly 50 times cheaper than Pt and reasonably active towards ORR.[8] However, the activity and stability of Ag based electrocatalysts is still poor compared to commercial Pt/C catalysts, which hinders their industrial application in air cathode of metal-air batteries.[9, 10] To address this issue, efforts have been spent on improving the activity and stability of silver by alloying. Recent studies have shown that the alloying of two metal within a nanoparticle with precise control over structures could lead to very important synergistic effects for potential application in catalysis and optics.[11-13] Cobalt, palladium, and nickel are typically used as doping elements in Ag-based catalysts.[3, 14-16] Compared to pure Ag, these alloyed silver catalysts have lower over-potential, and higher limiting current density along with durability during the battery charge-discharge tests. Although these alloy catalysts demonstrated an activity enhancement in ORR, they suffer significant alloying degree limitation due to the solubility of the Ag. For most of silver crystalline catalyst, the solubility limits the alloying elements at equilibrium, for example, the mutual solubility of Cu and Ag is less than 1 at% at room temperature. [17, 18] This limitations of solubility would greatly reduce the degree of alloying and hinder the performance of catalysts.

These solubility limitations could be eliminated if the amorphous alloy can be developed. Recently, researchers started thinking in catalyst materials with metallic glasses (MG) which are monolithic in phase and homogeneous in composition.[19, 20] Several immiscible alloy systems have demonstrated high solubility in the metallic glasses prepared via vapor-quenched method.[21-23] The metallic glasses can be more corrosion resistant than nanocrystalline catalysts,[7, 24] thus benefiting preventing catalysts to dissolve in the electrolyte and improve the stability of catalysts, such as Pd-Cu-Si and Pd-Ni-P. [25, 26, 27] Moreover, the amorphous phase is in metastable, in which the constituent atoms do not reside at the thermodynamic equilibrium positions, but locate in far-from-equilibrium states (corresponding to crystalline state).[28,

[a] State Key Laboratory of Solidification Processing, Northwestern Polytechnical University, Xian,710072,China
[b] Department of Chemistry, University of Birmingham, Birmingham, B15 2TT, U.K.
Electronic Supplementary Information (ESI) available: [TEM results of AgCu-MG catalyst, XRD results of AgCu-MG on glasses and nickel foam, Elements mapping of Ag and Cu on nickel foam, Koutecky-Levich plots, ORR polarization curves and CV curves of AgCu-MG, XPS results of AgCu-alloy patterns, Schematic of AuCu-MG based air electrode and rechargeable zinc-air batter].See DOI: 10.1039/x0xx00000x

[29] When dealloying/corrosion occurred on the surface of metallic glasses, these far from equilibrium states atoms are easy to introduce a realloying and protect the subsurface doping element atoms. Recent reports suggest that these subsurface doping elements can influence the electronic structure(d-band center) of the surface and improve the activity of the catalyst towards ORR.[2, 8] On the other hand, the metastable nature imparts many excellent properties to these restructuring metal glasses that are unachievable for crystalline alloys, such as Pd/CuO-TiO_2 prepared by a one-pot procedure that involved dealloying an amorphous Ti-Cu-Pd alloy;[30] nanoporous Cu prepared by dealloying amorphous Cu-Hf-Al-alloys[31] and homogeneous nanocrystalline Pt coatings with hierarchical pore structure by electrochemical dealloying of amorphous sputter-deposited platinum silicide layers. [32] In addition, following the process of dealloying on the catalysts, the restructuring processes (induced by potential) produce a refresh surface and form a mono- or bimetallic multilayer, which will enhance the activity of catalyst significantly(such as Ru(0001) surface).[33] Thus, amorphous structure and surface realloying play an important role in obtaining high activity and stability. Unfortunately, the metallic glasses derived from low-cost Ag based electrocatalyst for oxygen reduction (ORR) and evolution reaction (OER) have rarely been reported. However, few reports explain the surface dealloying phenomenon for activity and stability enhancement over AgCo and AgAl nanoparticles (crystalline alloys).[15, 34]

Herein, we describe a silver-copper metallic glass (AgCu-MG in short) prepared by pulsed laser deposition (PLD, a kind of vapour-quenched method) onto the nickel foam as a carbon-free, binder-free catalyst. The newly developed AgCu metallic glass catalysts is distinct from the Ag-based nano-crytalline catalysts in structure and properties. The composition of Ag and Cu is accurately controlled by PLD technology, which ensure the Ag atoms absolute alloyed. Simultaneously generating nanoparticles (mean size is 2.3 nm) together with amorphous film improves the stability of AgCu-MG film in ORR processes. After in-situ dealloying in 0.1M KOH, the AgCu-MG catalyst exhibits exceptionally excellent half-potential (0.78V vs.RHE), which is comparable to 0.81 V(vs.RHE) of Pt/C-20%. When applied this catalyst to direct primary Zn-air battery and recharge Zn-air battery, both of them showed exceptionally excellent activities and operation stabilities for charge-discharge process as compare with commercial Pt/C-20% cathode fuel cell. This AgCu-MG catalyst can be a promising replacement to the Pt-based electrocatalysts in alkaline fuel cells and metal-air batteries.

Experimental

Materials

Ag-Cu alloy (the rate of Ag to Cu is 1:1), Cu (99.99 wt%) and pure Ag (99.99 wt%) were used as sputtering target materials and the nickel foam (99.99%) was used as substrate. Acetylene black and Teflon (65%) were purchased from Lzydch. Absolute alcohol was purchased from Xi'an Shunda. The Pt/C-20% catalyst was purchased from Johnson Matthey Fuel Cell. Zn plate (99.995%) was purchased from Xinrixinye. The potassium hydroxide(KOH) and zinc acetate dihydrate(99.9%) were purchased from Tianjin Fuchen. Electrolyte solutions were prepared with deionized water.

Preparation of catalyst layer (CL)

The nickel foam was first cleaned in dilute sulphuric acid for 5min and soaked in acetone solution for 2 hours. After washing by deionized water and drying, the nickel foam was used as a substrate and set on an adjustable rotation rate sample platform (ARRSP) of the pulse laser deposition (PLD). AgCu sputtering target or pure Ag sputtering targets was fixed on an adjustable rotation rate target platform (ARRTP) of the PLD. Both the ARRSP and ARRTP were rotated at the speed of 6 rpm and cooled by flowing helium during the deposition process. The distance of the ARRSP -to- ARRTP is 12cm. To clearing the surface of the targets, nanosecond Q-switched Nd (YAG laser beam with a wavelength of 266 nm and a pulse duration of 3-6 ns, beam diameter was about 1 mm with an energy density 200 mJ/pulse, EKSPLA, Lithuania) was performed to irradiate the targets for 5 minutes at 2Hz. After this process, the $Ag_{50}Cu_{50}$ or Ag targets were allowed to deposit onto the nickel foam at 8 Hz. All of the catalyst patterns were deposited with 36000 laser pulses. To prepare the annealed patterns(AgCu-NC),the AgCu-MG catalyst(directly prepared by PLD) was heat treated at 300℃ for 2 hours in a vacuum chamber. For the rotating disk electrode (RDE) test, the catalyst layer was fixed to the surface of glassy carbon electrode(GC) by conductive copper tap and fix it by PARAFILM (purchased from BEMIS company). The area of the catalyst layer was 0.196 cm^2.

Preparation of gas diffusion layer (GDL)

0.5g of acetylene black, 2.5ml of PTFE (65%) and 15 ml of absolute ethanol was mixed with 5ml of deionized water and stirred for 3 hours to form a colloidal solution. This colloidal solution was separated in ultrasonic for 15minutes and bath heated in 80℃ water for 10 minutes to prepare the acetylene black colloid. The gas diffusion layer (0.4mm thick) was prepared by drying this colloid and static press at 10 MPa pressures for 30min.

Preparation of air electrode and Zn-battery

To prepare the air electrode, both the CL and GDL were rolled to thickness of 0.4mm and vacuum dryed for 30 min. The prepared GDL and CL were rolled them to 0.5mm and heated on a hot plate for 5 min. Finally, the electrode was cut to size (1 cm^2) for Zn-air battery. A Zn-air battery device was designed for the battery test. As shown in Figure S6, a single cell of homemade direct zinc-air battery was used for the performance test, a polished zinc plate (approximately 4 gram) was used as the anode electrode. AgCu-MG-based and AgCu-NC based air electrodes (area is 1 cm^2) were used as the cathodes. The catalyst loading was 0.112 mg. 6 M KOH

solution without and with 0.1M zinc acetate was employed as electrolyte in primary and rechargeable zinc-air battery respectively.

Microstructural Characteriszation

X-ray photoelectron spectroscopy (XPS) measurements were performed on an ULTRA (ESCALAB 250, Al Kα，ultrahigh vacuum is 10^{-9}， hv = 1486.6 eV). The data obtained are the typically of the samples. High-resolution O_{1s}, Cu_{2p} and Ag_{3d} spectra were acquired. No charge compensation was necessary. The origin of the binding energy E_b was set to the Fermi energy E_f of the Au plate. X-ray diffraction (XRD) and high-resolution transmission electron microscopy (HRTEM) were used for catalyst analysis. The surface morphologies and compositions of the synthesized catalysts were examined by transmission electron microscopy (TEM, FEI Tecnai F30) at 200 kV, scanning electron microscope (SEM) and quantitative energy dispersive spectroscopy (EDS).

Electrochemical testing

All electrochemical measurements were carried out by a classic three electrode set-up. The saturated calomel electrode (SCE) was used as a reference electrode(connected with KOH solution via salt bridge, whose solution is saturated KNO_3), a Pt wire electrode was employed as a counter electrode and the working electrode was fabricated by AgCu-MG, AgCu-NC, pure Cu and pure Ag catalyst layers. The rotating disk electrode (RDE) and CHI660C electrochemical workstation were performed to measure the electrocatalytic activity of the catalysts. The diameter of the RDE is 5mm and the active area is 3.14 x 0.25^2 cm^2 (approximately 0.196 cm^2). The linear voltammetry scanning (LSV), cyclic voltammetry(CV) and rotating disk electrode (RDE) polarization curves were studied at room temperature in 0.1M KOH(O_2 saturated). The experiments were performed over the potential range of 0 to -0.8 V at a scanning rate of 10 mV s^{-1} and the rotation rates were controlled at 400, 900, 1600 and 2500 rpm. The primary Zn-air battery was fabricated by the air electrode (1 cm^2), zinc plate and an alkaline electrolyte (6.0 M KOH aqueous solutions). The alkaline electrolyte for secondary Zn-air battery is the aqueous solutions contain 6.0 M KOH and 0.1 M $Zn(CH3COO)_2$. The performance of the zinc-air batteries were measured and recorded by a TC 5X battery testing system (Neware Company, Shenzhen) at atmosphere in the air. Battery testing and cycling experiments were performed at 25°C at 1 atmosphere.

Results and discussion

High-resolution TEM (Figure 1a), selected area electron diffraction (Figure 1b), and the XRD pattern (Figure 1c) indicated that a dense amorphous structure of the AgCu alloy was formed. Figure 1a shows that there is no periodic microstructure observed on the whole surface except one striking feature, that is, a few cluster ranging from 1 nm to 5 nm were visible in the HRTEM images with the interplanar spacing around from 0.230 nm to 0.236 nm, which can be indexed to the Ag(111) facet. This TEM images of AgCu

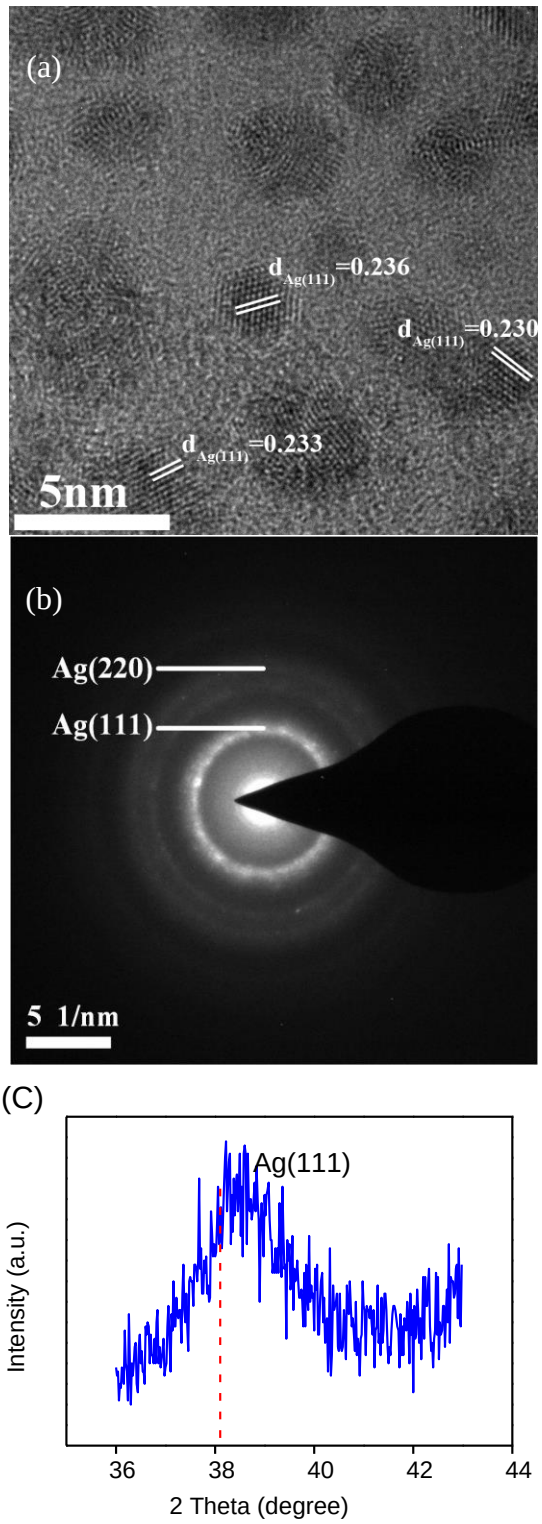

Figure 1. (a) HRTEM images of the AgCu-MG, (b) Selected area electron diffraction (SAED) of the AgCu-MG, (c) X-ray diffraction patterns of the AgCu-MG on nickel foam.

metallic glass is reported for the first time and is different with the heterogeneously granular structure with nano-particles in Au nano-glass catalyst.[35] The selected area electron diffraction pattern (in Figure 1b and Figure S2) shows only diffuse haloes, implying that the alloys are glassy. The X-ray diffraction pattern (in Figure 1c and Figure S3) displays a broad diffraction maximum with no observable crystalline peaks confirming the amorphous nature of the alloy. As showed in Figure S4, we further deposited the AgCu alloy on a plain glass slip, these XRD patterns also present a single broad peak far away from the Ag(111) face at 2θ =39°, which indicated these alloys are in an amorphous nature. It should be noted that these experimental observation is agreeable to a previous simulation that a laser-induced glass is formed in $Ag_{60}Cu_{40}$ alloy.[36] For the application in air-cathode, AgCu metallic glass catalyst was deposited on the nickel foam to form a continuous and smooth surface as shown in Figure S4. Elements mapping reveals that the Cu and Ag are uniformly distributed on the collector electrode.

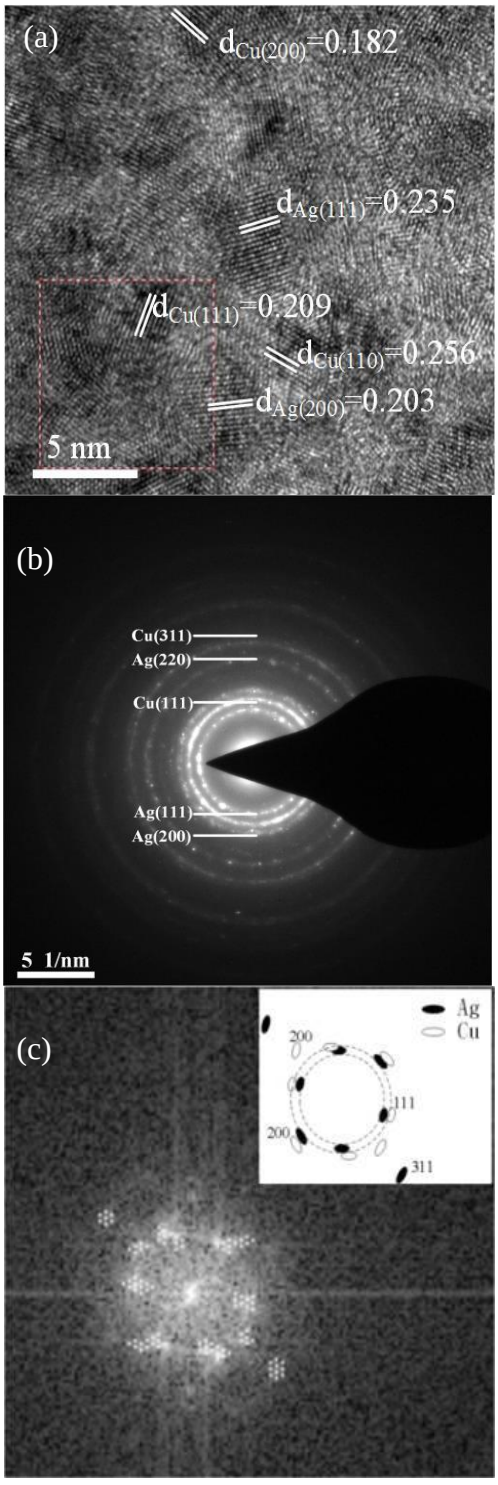

Figure 2. (a) HRTEM images of the AgCu-NC, (b) SAED of the AgCu-NC, (c) Fast Fourier Transformation (FFT) diffraction pattern and its schematic drawing for AgCu-NC.

The silver-copper nanocrstalline (AgCu-NC in short) catalysts were fabricated by in-situ annealing of AgCu-MG catalysts at 300 °C in PLD furnace, their morphology and structure were shown by the high-resolution TEM in Figure 2a, their crystalline nature was further analyzed by the selected area electron diffraction pattern (SAED) in Figure 2b and a Fast Fourier Transform (FFT) diffraction pattern in Figure 2c. As shown in Figure 2a, plenty and bigger crystal facets are displayed on the surface in comparison to the AgCu metallic glass catalyst, suggesting a higher degree of crystallinity. The lattice fringes with an interplanar spacing of 0.235 and 0.209 nm correspond to the Ag(111) and Cu(111) planes of fcc pure Ag and Cu metal, which indicate that the nanocrystalline catalysts were formed by a phase separation during annealing process of metallic glass. The phases in AgCu nanocrystalline catalysts were further measured by SAED as shown in Figure 2b, which present sharp diffraction rings of Ag(111), Cu(111), Ag(200) and Cu(200) with agreeable interplanar spacing to HRTEM images. These diffraction rings may come from the Ag-rich or Cu-rich fcc solid solution phase.[37,38] This result is in consistent with F.Misjak's report suggest the Ag or Cu is not purity, which is an Ag-rich phase (with ~1at.% Cu) or Cu-rich phase (with ~1at.% Ag).[18] Figure 2c shows the FFT pattern corresponding to the 8*8 nm^2 region of Figure 2a, the two phase nature of Ag and Cu crystallites are obviously present in an epitaxial relationship relative to each other. Schematic diagram of this FFT in inset of Figure 2c reveals that the two fcc of Cu and Ag lattices are parallel along the equivalent direction of <111> and <200>.

To investigate and compare ORR activities of the AgCu metallic glass and nanocrystalline catalysts, we conducted line sweep voltammetric (LSV) measurements in O_2-saturated 0.1M KOH solution using a rotating disk electrode (RDE), as shown in Figure 3a. Clearly, the metallic glass and nanocrystalline catalysts exhibited a more positive on-set potential and higher limited current density than those of the pure Ag or Cu catalysts. Moreover, the half-wave potential $E_{1/2}$ increased in the order of pure Ag, AgCu-NC and AgCu-MG catalysts. The enhanced $E_{1/2}$ in AgCu alloy catalyst is clear in contrast to pure Ag, a similar ORR activity enhancement was

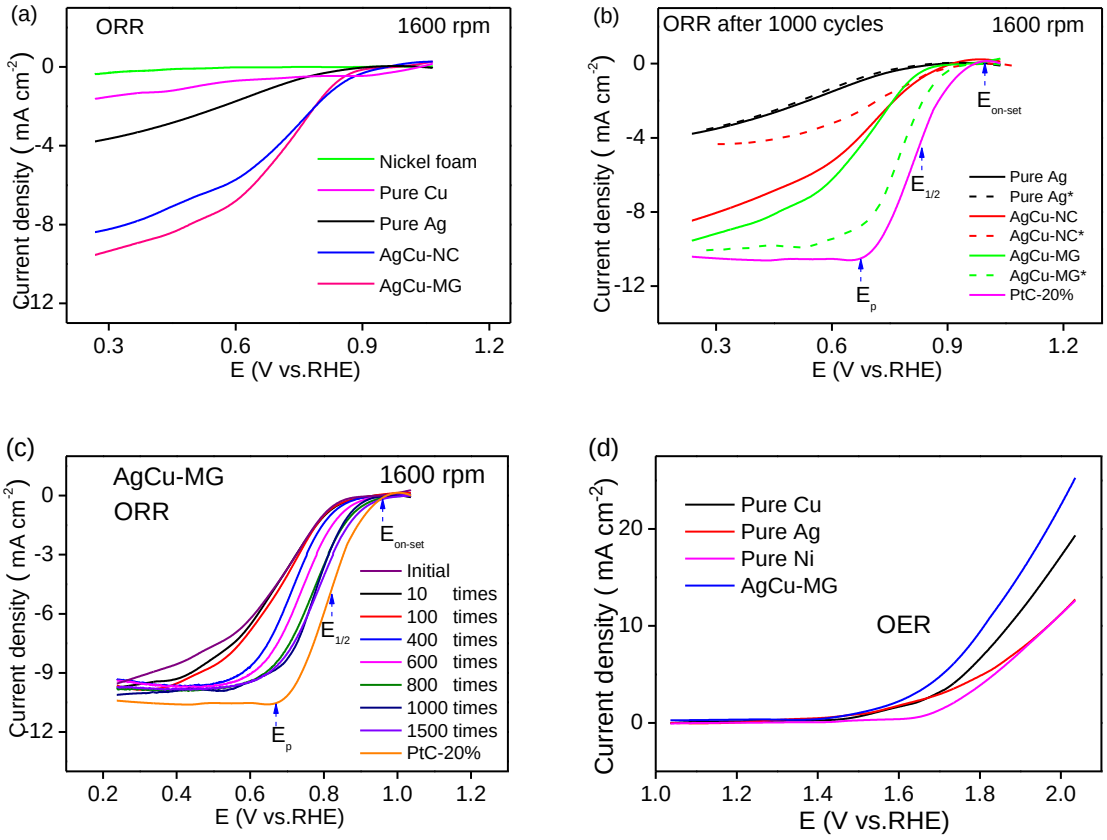

Figure 3. (a) ORR polarization curves of the AgCu-NC, AgCu-MG and refernece catalysts in O_2 saturated 0.1M KOH solution, (b) ORR polarization curve before and after 1000 CV cycle treatments for the AgCu-NC, AgCu-MG, referrence catalysts and Pt/C-20%, solid lines depict the samples before CV test, dash lines and asterisk (*) depict the corresponding samples after 1000 CV cycle treatments, (c) ORR polarization curve for the initial, 10,100,300,500,700 and 1000 CV voltammetric treatments for the AgCu-MG catalysts, (d) Linear sweep voltammogram (LSV) displaying oxygen evolution activities of AgCu-MG， pure Ni, pure Cu and pure Ag electrodes.

reported for the Ag-Co alloy by Holewinski where the Ag catalysts is alloyed with Co element,[3] however, there is little difference in ORR activity between AgCu nanocrystalline and metallic glass catalysts.

We next measured the stability of the AgCu-MG and AgCu-NC catalysts in ORR process via cyclic voltammetry accelerated stability test (AST), that is, continuously applying CV to characterize the ORR performance of these catalysts for 1000 times cycle. The ORR activity of AgCu metallic glass catalyst is increased after AST test, as shown in Figure 3b, the half-wave potential (marked as $E_{1/2}$ in the dotted green curve) shifted positively by about 0.11 mV from 0.67 V to 0.78 V(vs. RHE). For AgCu-NC, the $E_{1/2}$ decayed about 0.21 mV from 0.69 V(vs. RHE) as expected. These results suggest the AgCu-MG catalysts present superior stability than AgCu-NC catalysts. It is noteworthy that the activity with $E_{1/2}$ of 0.78V (vs. RHE) for AgCu-MG catalyst after 1000 CV cycles is close to the activity reported for Pt/C-20wt%. i.e. $E_{1/2}$ of 0.81V(vs. RHE) Further study from the AST measurement is shown in Figure S6(a-c), these results confirmed the results of Figure 3b. Figure S4e, S4f and 3c show the RDE polarization curve of AgCu metallic glass catalyst before and after 1000 CV cycle (labelled as AgCu-MG or AgCu-MG*, respectively)at different rotation rates, the number (n) of electrons transferred in the ORR process is obtained from the slope of the Koutecky-Levich plot, as shown in Figure S4d, at the potential of 0.3 V (vs. RHE), the electron transfer numbers (n) of AgCu-NC and AgCu-MG catalysts is 3.8 and 4, respectively, also indicating the ORR rate of AgCu-MG catalyst is enhanced by AST process. The OER activities of the nickel foam, AgCu-MG, pure Cu and pure Ag electrodes are shown in Fig. 3(d). As shown, the AgCu-MG exhibits higher OER current density than pure Ni at 1.9V (vs.RHE), and displays lower onset potential than nickel foam, suggesting that the OER is enhanced by Ag-Cu alloy. Compared to the OER performance of pure Ag and Cu, the Ag-Cu alloy also have a better OER performance, indicating the OER activity of Ag is also enhanced by alloying with Cu.

To further understand why these AgCu-MG catalysts are more stable than the AgCu-NC catalysts, we carried out X-ray photoelectron spectroscopy (XPS). Previous work indicated that the oxidation and dissolution of less-noble or base metal elements are believed to be major deactivation role of Ag-based alloy systems and that the factors affecting Ag and Cu oxidation resistance usually contains very complex surface

Table 1. The surface composition of the AgCu-MG, AgCu-NC, AgCu-NC* and AgCu-MG* measured by XPS-0° and EDS.

Surface composition	XPS-0° analysis 2 nm near-surface composition (at.%)		XPS-0° analysis 10nm surface composition (at.%)		EDS analysis catalyst layer composition,(at.%)	
	Ag	Cu	Ag	Cu	Ag	Cu
AgCu-MG	31.1	68.9	29.4	70.6	42.5	57.5
AgCu-MG	31.8	68.2	29.8	70.2	47.3	52.7
AgCu-MG	29.9	70.1	29.7	70.3	45.6	54.4
AgCu-MG*	70.2	29.8	56.7	43.3	48.5	51.5
AgCu-NC	35.7	64.3	32.1	67.9	52.6	47.4
AgCu-NC	39.4	60.6	35.9	64.1	48.5	51.5
AgCu-NC	40.3	59.7	31.4	68.6	42.1	52.9
AgCu-NC*	100	0	100	1.2	95.7	4.3

* The AgCu alloy is exposed to the 1000 CV cycle treatments in 0.1M KOH solution.

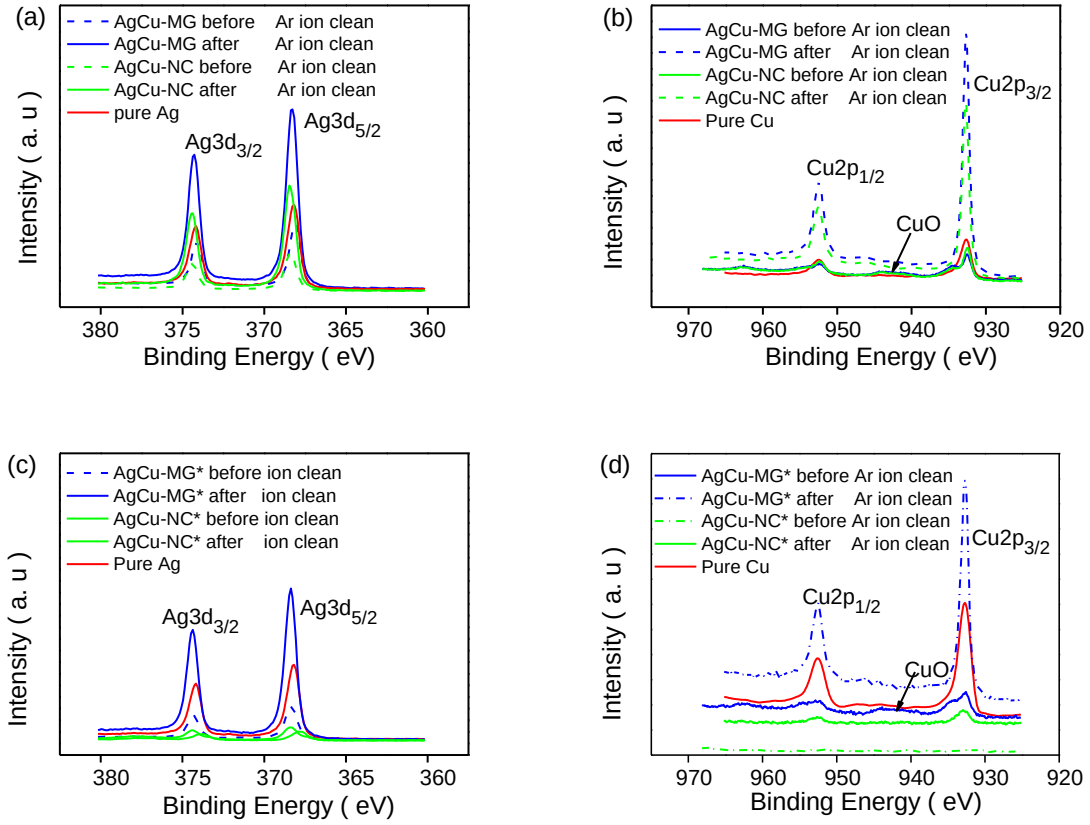

Figure 4. (a) XPS spectra of Ag, Cu and AgCu catalysts before or after ion clean:(a) Ag 3d regions of AgCu-NC, AgCu-MG and Ag, (b) Cu 2p regions of AgCu-NC, AgCu-MG and Cu, (c) Ag 3d regions of AgCu-NC*, AgCu-MG* and Ag, (d) Cu 2p regions of AgCu-NC*, AgCu-MG* and Cu.

segregation,[3] phase composition and microstructure.[39] To measure the ability of Ag and Cu elements resist oxidation in AgCu-MG and NC catalysts, high resolution X-ray photoelectron spectroscopy(XPS) analysis was conducted. Figure.4a and Figure.4b present the XPS pattern of the surface of Ag, AgCu-MG and AgCu-NC which were fully exposed in air for 20 hours before XPS measurement, the XPS peaks of Ag element at 368.27 and 374.37 eV can be attributed to metallic silver (Figure 4a), the XPS peaks of Cu element at 952.47 and 932.67 eV are assigned to Cu $2p_{3/2}$ and Cu $2p_{1/2}$ of metallic Cu, the satellite peak at 942eV is from the oxidized Cu atoms on surface of AgCu-MG and AgCu-NC (Figure 4b). These experimental compares show that Cu atoms are more easily oxide than Ag atoms on AgCu-MG and AgCu-NC surface. The satellite peak of the oxidized Cu atoms disappeared after Ar ion etching for 15 seconds or 2 nm depth, indicating that the oxidation occurred on the surface. Figure S5a shows the full survey scan before and after Ar ion etching for the Ag, AgCu-

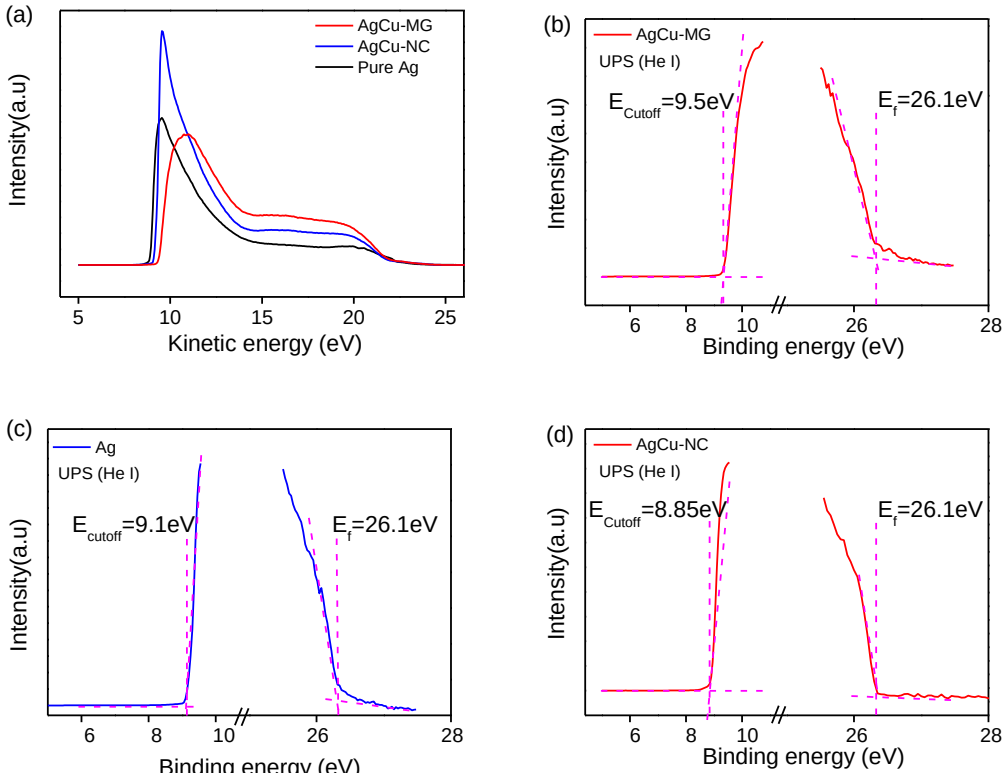

Figure 5. (a) Ultraviolet photoelectron spectroscopy (UPS) spectra of AgCu-MG, AgCu-NC and Ag layers on nickel foam substrate, (b) corresponding E_{cutoff} and E_f states of AgCu-MG, (c) corresponding E_{cutoff} and E_f states of Ag, (d) corresponding E_{cutoff} and E_f states of AgCu-NC.

MG and AgCu-NC samples, there are no nickel peaks at 853 and 870 eV, indicating that the Ag and AgCu film fully cover the surface of nickel foam during PLD.

The oxidized Cu atoms in catalysts can lead to two opposite roles in ORR process, one is to form a passivation coating on catalyst surface to prevent the Cu atoms from dissolving in alkaline solution and the second is that the oxidized Cu atoms dissolve in alkaline solution to dealloy the bimetallic catalysts seriously. Regarding this point, we measure the XPS pattern of the surface of Ag, AgCu-MG and AgCu-NC after 1000 times CV cycle, where the correspoding samples are labelled as Ag*, AgCu-MG* and AgCu-NC*. Table 1 lists the Ag and Cu compositions in the catalyst layer before and after Ar ion etching as measured by high resolution XPS (HR-XPS). Figure S5b shows the full survey scan before and after Ar ion etching for the Ag*, AgCu-MG* and AgCu-NC* samples. It is indicated that the AgCu-NC* catalyst after CV cycles presents two Ni2p peaks at 853 and 870eV in full survey and no Cu2p peaks were observed at 952.47 and 932.67 eV, which indicated the AgCu-NC catalyst layer is thinned and the Cu atoms is dissolved from it during CV cycles. After etching with Ar ion for 90 seconds (approximately 10 nm depth into the catalyst layer), two weak Cu 3p peaks appear in its XPS curve and the percentage of Cu is about 1.2%, as shown in Table 1. These results confirmed the Cu atoms in AgCu-NC dissolved in alkaline solution which led to the unstable catalytic performance as shown in Figure 3b. For AgCu-MG* sample, the Ag3d peaks in Figure 4c shows that the surface Ag atoms on AgCu-MG* are stable and have no oxides, the Cu 3p peaks in Figure 4d indicate the surface Cu atoms are oxidized in ORR process. After Ar ion etching for 90 seconds, the satellite peak of Cu element disappeared, which suggests that the Cu oxides on the surface of AgCu-MG* catalyst layer protected the inner Cu atoms from dissolving and enhanced the ORR stability of the AgCu-MG catalysts.

We further compared the changes of the film composition as well as near-surface composition of the AgCu-MG and AgCu-NC catalysts after 1000 times CV cycle, as shown in Table 1. Composition analysis for the AgCu-MG and AgCu-NC showed that the have no apparent changing in bulk compositions, however, after 1000 times CV test, the Cu content on AgCu-NC surface is reduced from 51.5% to 4.3%, and the composition of Cu in AgCu-MG surface is almost the same. The XPS-0° analysis show that the Cu content on AgCu-NC surface with depth of 2 nm is close to 0%, the Cu content AgCu-NC surface with depth of 10 nm is closed to 0% too. In comparison, the Cu content on AgCu-MG surface is 29.8% after 1000 times CV test, the Cu content AgCu-MG surface with depth of 10 nm is closed to 43.3%. These results indicated the inner Cu atoms on AgCu-NC surface were dissolved during CV test. This phenomena is understandable, as shown in Figure 2, the AgCu-NC catalysts have a phase separation [17, 40] of Ag-rich and Cu-rich phase, in which the Cu rich phase are dissolved preferentially in alkaline

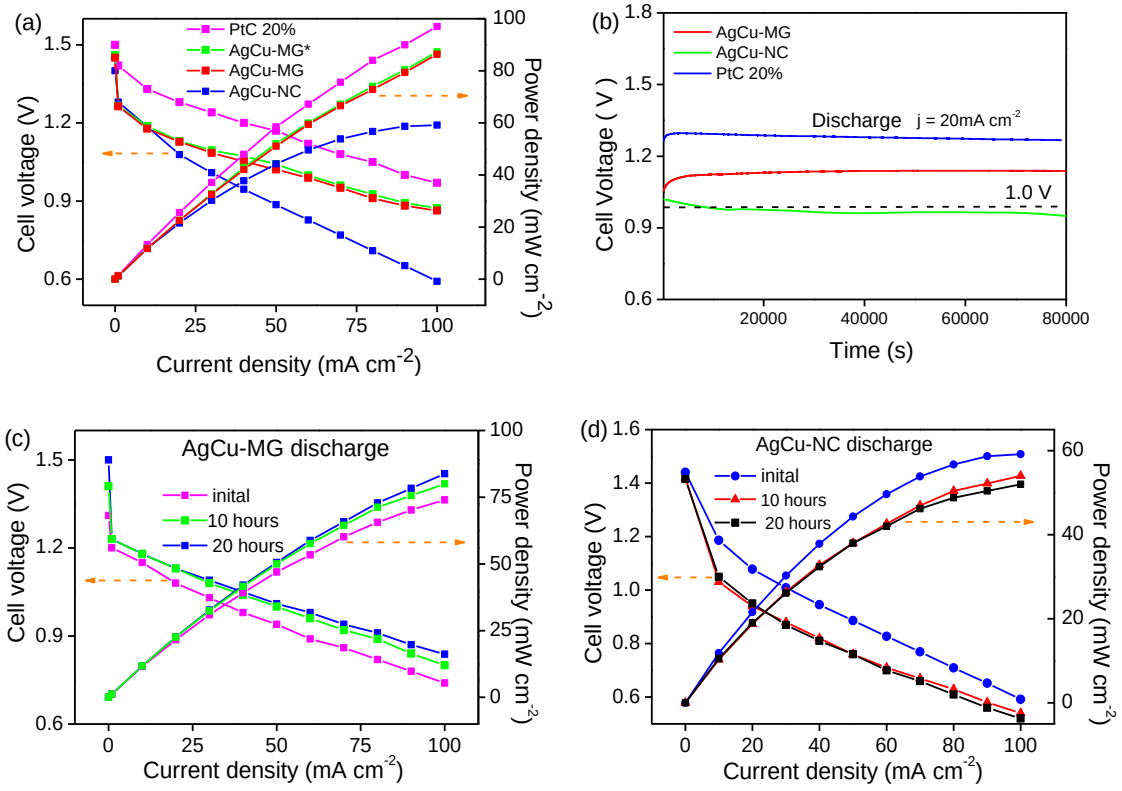

Figure 6. (a) The discharge polarization and power density curves for AgCu-MG, AgCu-MG*, AgCu-NC, and PtC-20% based catalyst layers of the primary zinc-air battery, (b) The galvanostatic discharge curves of the primary zinc-air battery at 20 mA cm^{-2} for AgCu-MG, AgCu-NC, and PtC-20% catalysts. (c) The discharge polarization and power density curves for AgCu-MG after discharged for 10 and 20 hours. (d) The discharge polarization and power density curves for AgCu-NC after discharged for 10 and 20 hours.

solution, but the amorphous structure in AgCu-MG surface is homogeneous which prevents the corrosion to proceed. To help understand these results, we determined work function (Φ) of electron on the surface of AgCu, which is necessary to understand the influence of electronic perturbation on Ag based catalyst's stability; however, there are numerous unresolved questions and a lot of influences. Given the nature of AgCu alloy, the work function (Φ) is one of relevant for AgCu alloy to capture electron, which influence the corrosion resistant capacity of alloys.[41, 42] We conducted ultraviolet photoelectron spectroscopy (UPS) measurement to estimate the work function of AgCu-MG, AgCu-NC and Ag. The work function measurements enable us to directly correlate the catalytic stable with electronic perturbation in AgCu-MG, AgCu-NC and Ag. The ϕ is determined from the following equation:[43]

$$\Phi = h_v + E_{cutoff} - E_f \qquad (1)$$

where ϕ is work function (21.2eV), h_v is the energy of the UV photon, E_{cutoff} is the energy of the final state, E_f is the Fermi energy or the energy of the initial state. As shown in Figure 5 the energy of the initial state of AgCu-MG, AgCu-NC and Ag is the same(26.1eV); but for the energy of the final state, the E_{cutoff} is in the order of AgCu-MG > Ag > AgCu-NC. From equation 1, the Ag the Φ of AgCu- MG (4.6eV) and Ag (4.1eV) are higher than AgCu-NC (4.2eV), indicating the amorphous structure of AgCu-MG increased the energy of loses electronics which is helpful to protect Cu from the corrosion of alkaline solution. The high ORR stability of AgCu-MG catalysts can be understood in terms of the geometrical effect. The AgCu-MG surface has a high Cu content even after 1000 times CV test, the Cu-doping atoms influence the electronic structure of Ag-based catalysts, that is, the increasing of Cu atoms in Ag-Cu will positively shift the d-band center to Fermi energy, increase the binding energy of O_2 molecule to the catalyst surface, and finally improve their ORR activity.[3, 44]

To further study the activity and stability of AgCu catalysts in real battery operation conditions, a primary zinc-air battery was constructed, as shown in Figure S6, in which an air electrode was prepared by coating the gas diffusion layer (GDL) on the nickel foam, followed by pulse laser deposition of AgCu catalysts (0.112 mg) on the electrode. The 6M KOH electrolyte was filled between the cathode and anode made by zinc metal plate. The discharging polarization curves in Figure 6a and the galvanostatic discharge curves in Figure 6b reveal that the performance of AgCu-MG-based batteries are superior to the AgCu-NC-based batteries. The AgCu-MG-based batteries illustrate an open circuit voltage of 1.45V, a high current density of 49.96 mA cm^{-2} at 1.0V and the power density improved to 86.6 mW cm^{-2} when discharged at 100 mA cm^{-2}, which are comparable to those previously reported

catalysts including Ag/C, MnO_2 and MnO_2/Co_3O_4[6, 45, 46 9, 38, 39]. Although, the discharge performance of AgCu-MG based Zn-air batteries are slightly lower than that of primary zinc-air batteries, whose power density is from 100 to 110 mW cm^{-2} at 100 mA cm^{-2} as catalyzed by amorphous MnO_x nanowires and FeCo-EDA catalysts,[48,49] our zinc-air batteries can be further improved for their charge-discharge performance. For the AgCu-NC-based batteries, the curves present a similar discharge voltage of 1.2 V at low current density of 10 mA cm^{-2}, but a poor polarization in high current density from 20 to 100 mA cm^{-2}. In contrast with the performances of the commercial Pt/C-20% with loading of 1.2 mg cm^{-2}, the AgCu-MG-based batteries shows voltage plateau of 1.14 V at the current density of 20 mA cm^{-2}, which is comparable to present Pt/C–based batteries (1.26 V) and slightly higher than the previously reported one (1.10 V).[47] It is noteworthy that the loading of AgCu-MG used in this work is only 0.112 mg, which is much lower than that of Pt/C system.

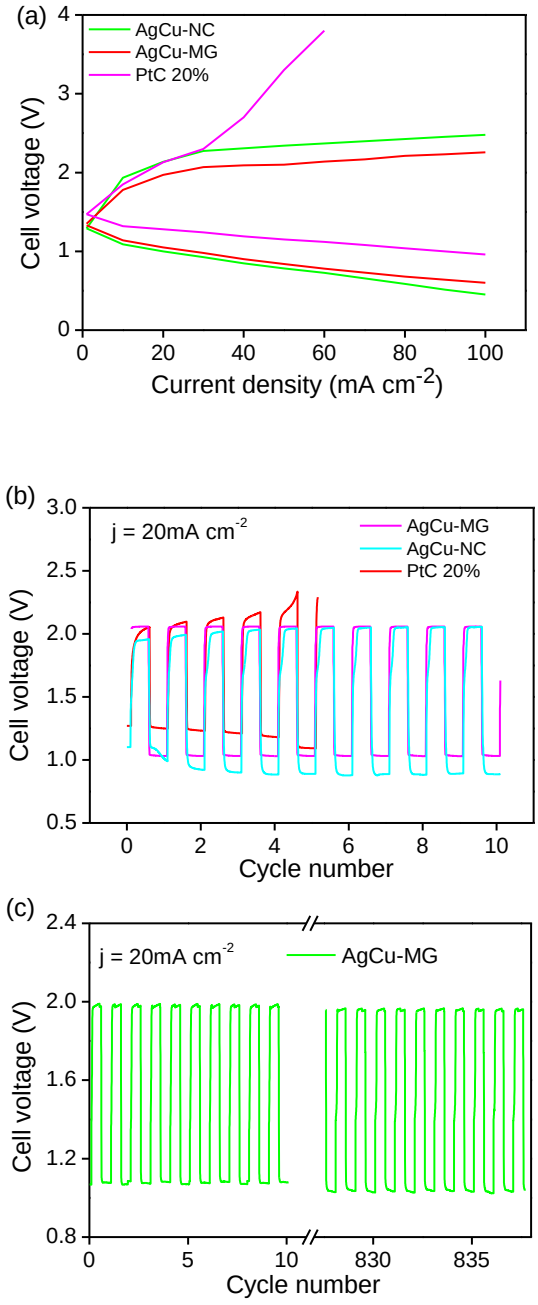

Figure 7.(a) The charge-discharge polarization curves of the AgCu-NC, AgCu-MG and PtC-20% based rechargeable zinc-air battery, (b) The first-ten cycles of the AgCu-NC, AgCu-MG and PtC-20% based rechargeable zinc-air battery with period of 1800s, (c) long-term cycle of rechargeable Zinc-air battery.

We further studied the activity of AgCu catalysts after a period of galvanostatic discharge to observe the stability of AgCu catalyst in operation. Figure 6c and Figure 6d show the discharging polarization curves for AgCu catalytic zinc-air battery used after 10 and 20 hours discharging at 20mA cm^{-2}, only a slight voltage drop is observed for the MG catalysts, whose cell voltage was approached to 0.82V, and the power density was reduced 5 mW cm^{-2} at 100mA cm^{-2} after discharging for 20 hours. For AgCu-NC catalytic zinc-air battery, the cell voltage was reduced to 0.52V and the power density was reduced approximately 7.15 mW cm^{-2} at 100mA cm^{-2} after discharging for 20 hours. It should be noting in Figure. 6(c), AgCu-MG based Zn-air battery exhibited a higher discharge voltage after discharging for 10 hours. To further understand this phenomenon, we carried out XPS to measure the surface composition and electronic state of the AgCu-MG catalyst. As shown in Figure S6b, the XPS-0° composition analysis reveals that the Cu oxides have appeared and the area of metallic Cu peaks is decreased after discharge for 10 hours, it can be concluded that the Cu content of surface in the AgCu-MG catalysts is decreased after charge-discharge cycle, indicating the AgCu metallic glass catalyst undergoes in situ dealloying on the bimetallic surface, which further promote the ORR performance due to the geometric effect.

The stability of the AgCu catalysts were also investigated in rechargeable zinc-air batteries using the same construction except for adding 0.1M zinc acetate to 6M KOH electrolyte, where zinc acetate is benefited for the zinc plate anode during the reversible recharging process. The period or time per cycle is 12 minutes during the 1000 cycles in rechargeable Zinc-air battery the same as in Figure. 7b and Figure. 7c. In the case of the AgCu-MG cathode, the sum of charging and discharging over-potential is 1.20V at a current density of 50 mAcm^{-2}, as shown in Figure 7a, this value is significantly lower than that measured with AgCu-NC (1.75V) and the Pt/C cathode.[47] Notably, during long-term charge–discharge cycling tests using a constant current density of 20 mAcm^{-2}, the AgCu-MG cathode in rechargeable zinc–air batteries shows the highest round-trip efficiency (negligible voltage change at the end) and the smallest sum of over-potential (0.86V) when compared with AgCu-NC cathodes, as shown in Figure 7b. The AgCu-MG cathode presents almost the same discharge voltage of 1.1V at 20 mA cm^{-2} during the first four cycles, but the AgCu-NC cathode shows a discharge voltage of 0.9V at the fourth cycle.

This result is concomitant with results of CV cycles and confirms the separation of Cu-rich and Ag-rich phase after annealing at 300°C in AgCu-NC catalyst which affects its stability and performance. Compared to AgCu-MG cathode, the Pt/C-20wt% catalysts on carbon paper have about 0.1V higher discharging voltages and 3mW cm^{-2} higher power densities, but the cyclic performance of Pt/C-20% cathode was noticeably deteriorated after the fourth cycle. It is clear from these results that the AgCu-MG catalyst is an efficient bifunctional catalyst with substantially improved stability and minimized overpotentials during the discharging and charging processes.

A long-term discharge–charge cycling of two-electrode chargeable zinc–air batteries based on AgCu-MG catalysts is shown in the Figure 7c and Figure S7. Notably, we used ambient air, instead of pure O_2, which is more relevant to practical applications. As shown in Figure S7a, the discharge voltage at 20 mA cm^{-2} of AgCu-MG electrode increases from 0.9 to 1 V during the initial structure stable process of the cathode, and then stays at 1.1V after 400 cycles, indicating that the ORR activity of cathode catalyst is enhanced after tens of cycles. It is inferred that during structure stable process of the cathode, the AgCu metallic glass catalyst undergoes in situ dealloying or realloying on the bimetallic surface, similar enhancement of ORR activity also be reported in Pt-based bulk metallic glass system via dealloying.[50] The dropped voltage at 520th cycle is caused by changing the zinc plate anode. After 900 charge-discharge cycles, the discharge voltage begins to drop and reaches to 1.0V at 1200th cycle, which could be attributed to the passivation of the zinc anode.[13] As shown in Figure S7d, when the zinc anode and electrolyte were replaced, the AgCu-MG catalyzed cathode reactivated in a new zinc-air battery without significant voltage loss compared to the first cycle. Figure S7c shows the statue of the AgCu-MG catalysts after charge-discharge cycle 1200 times, it is clear that the nanostructure remains stable on the surface. The deteriorated voltage at 520th cycle is caused by the broken zinc plate (Figure.S7b). After changing new zinc plate, the battery continue cycling as before.

Conclusions

In this work, we have fabricated AgCu metallic glass electrocatalysts for ORR, and performed a systematic activity and stability investigation of AgCu metallic glass catalysts via TEM, SEM, XRD and XPS. This silver-copper metallic glass catalysts can in-situ dealloying via 1000-times CV treatment in 0.1M KOH and displayed good activity with a half-potential of 0.78V(vs.RHE), which is comparable to commercial Pt/C-20% catalysts. The AgCu nanocrstalline catalysts (annealed at at 300 °C) exhibits lower stability for ORR, after 1000 times CV the $E_{1/2}$ decayed about 0.21 V from 0.69 V(vs. RHE) as expected. But for AgCu metallic glass the $E_{1/2}$ increased about 0.11 V from 0.67 V to 0.78V (vs. RHE). Composition present the Cu atoms in the AgCu metallic glass is more stable than AgCu nanocrstalline catalysts by forming passivation layer to protect the interior Cu atoms. The AgCu metallic glass can retain more Cu atoms (about 43.3%) after 1000 times CV, which ensured the bimetallic alloying to enhance the stability of AgCu metallic glass. By directly using AgCu metallic glass in primary zinc-air batteries, it exhibited higher peak power density (86.6 mW cm^{-2}) at 100mA cm^{-2} and lower discharging polarization(5mW cm^{-2}) than AgCu nanocrstalline catalysts (7.15mW). When discharge at the current density of 20 mA cm^{-2}, the primary battery posses 1.14 V voltage and stable discharge 22hours without decay, which is comparable to Pt/C-20% (1.26V). For zinc-air batteries, the AgCu metallic glass catalyst present excellent activity and charge-discharging stability, after more than 800 charge-discharge cycles at current density of 20mA cm^{-2}, the battery's discharge voltage is kept at 1.0V, demonstrating a superiors performance to replace Pt/C (decayed after 5 charge-discharging cycles)based air cathodes.

Acknowledgements

This study was supported by the National Natural Science Foundation of China (grant nos. 51271148 and 50971100), the Research Fund of State Key Laboratory of Solidification Processing in China (grant no. 30-TP-2009), the Aeronautic Science Foundation Program of China (grant no. 2012ZF53073), the Science and Technology Innovation Fund of Western Metal Materials (grant no. XBCL-2-11) and the Doctoral Fund of Ministry of Education of China (grant no. 20136102110013).

Notes and references

1 Z. D. Wei, W. Z. Huang, S. T. Zhang and J. Tan, *J. Power Sources*, 2000, **91**, 83-85.
2 S. J. Hwang, S. K. Kim, J. G. Lee, S. C. Lee, J. H. Jang, P. Kim, T. H. Lim, Y. E. Sung and S. J. Yoo, *J. Am. Chem. Soc.*, 2012, **134**, 19508-19511.
3 A. Holewinski, J. C. Idrobo and S. Linic, *Nat. chem.*, 2014, **6**, 828-834.
4 J.-S. Lee, S. Tai Kim, R. Cao, N.-S. Choi, M. Liu, K. T. Lee and J. Cho, *Adv. Energy Mater.*, 2011, **1**, 34-50.
5 Y. Wang, Y. Liu, X. J. Lu, Z. P. Li, H. N. Zhang, X. J. Cui, Y. Zhang, F. Shi and Y. Q. Deng, *Electrochem. Commun.*, 2012, **20**, 171-174.
6 J.-J. Han, N. Li and T.-Y. Zhang, *J. Power Sources*, 2009, **193**, 885-889.
7 K. S. Suslick, S. B. Choe, A. A. Cichowlas and M. W. Grinstaff, *Nature*, 1991, **353**, 414-416.
8 K. Shin, H. Kim da and H. M. Lee, *ChemSusChem*, 2013, **6**, 1044-1049.
9 C. W. Chen, Y. S. Hsieh, C. C. Syu, H. R. Chen and C. L. Lee, *J. Alloys Compd.*, 2013, **580**, S359-S363.
10 P. Singh and D. A. Buttry, *J. Phy. Chem. C*, 2012, **116**, 10656-10663.
11 Y. C. Jin and F. Y. Chen, *Electrochim. Acta*, 2015, **158**, 437-445.
12 Y. M. Lei, F. Y. Chen, Y. C. Jin and Z. W. Liu, *Nanoscale. Res. Lett.*, 2015, **10**.

13 Y. Jin, F. Chen, Y. Lei and X. Wu, *ChemCatChem*, 2015, n/a-n/a.
14 D. A. Slanac, W. G. Hardin, K. P. Johnston and K. J. Stevenson, *J.Am. Chem. Soc.*, 2012, **134**, 9812-9819.
15 A. Holewinski, J. C. Idrobo and S. Linic, *Nat. chem.*, 2014, **6**, 828-834.
16 X. J. Song and D. M. Zhang, *Energy*, 2014, **70**, 223-230.
17 H. Chen and J. M. Zuo, *Acta. Materialia.*, 2007, **55**, 1617-1628.
18 F. Misjak, P. B. Barna and G. Radnoczi, *Thin. Solid. Films*, 2010, **518**, 4247-4251.
19 M. Pisarek, M. Janik-Czachor, A. Molnar and B. Rac, *Electrochim. Acta*, 2005, **50**, 5111-5117.
20 Z. Z. Chen, Y. Y. Yang, S. Kumar and G. Lu, *J. Phys. Chem. C*, 2014, **118**, 28609-28615.
21 S. Ningshen, U. K. Mudali, R. Krishnan and B. Raj, *Surf. Coat. Tech.*, 2011, **205**, 3961-3966.
22 S. J. Chung, A. Roy, D. H. Hong, J. P. Leonard and P. N. Kumta, *Mater. Sci. Eng.*, 2011, **176**, 1690-1694.
23 J. Paillier, R. Dolbec, M. A. El Khakani and L. Roue, *J. Alloys Compd.*, 2003, **358**, 126-132.
24 K. L. Edwards, E. Axinte and L. L. Tabacaru, *Mater. Des.*, 2013, **50**, 713-723.
25 L. Liu and B. Liu, *Electrochim. Acta*, 2006, **51**, 3724-3730.
26 Y. Yang, T. A. Maark, A. Peterson and S. Kumar, *Phys. chem. chem. phys. : PCCP*, 2015, **17**, 1746-1754.
27 M. Zhao, K. Abe, S. Yamaura, Y. Yamamoto and N. Asao, *Chem. Mater.*, 2014, **26**, 1056-1061.
28 A. L. Greer, *Science*, 1995, **267**, 1947-1953.
29 C. J. Byrne and M. Eldrup, *Science*, 2008, **321**, 502-503.
30 W. C. Xu, S. L. Zhu, Z. Y. Li, Z. D. Cui and X. J. Yang, *J. Power Sources*, 2015, **274**, 1034-1042.
31 Z. F. Wang, J. Y. Liu, C. L. Qin, L. Liu, W. M. Zhao and A.Inoue,*Intermetallics*, 2015, **56**, 48-55.
32 R. Kraehnert, E. Ortel, B. Paul, B. Eckhardt, M. Kanis, R. Liu and A. Antoniou, *Catal. Sci. Technol.*, 2015, **5**, 206-216.
33 A. K. Engstfeld, J. Klein, S. Brimaud and R. Behm, *Surf. Sci.*, 2015, **631**, 248-257.
34 Y. Zhou, Q. Lu, Z. B. Zhuang, G. S. Hutchings, S. Kattel, Y. S. Yan, J. G. G. Chen, J. Q. Xiao and F. Jiao, *Adv. Eng. Mater.*, 2015, **5**.
35 J. Q. Wang, N. Chen, P. Liu, Z. Wang, D. V. Louzguine-Luzgin, M. W. Chen and J. H. Perepezko, *Acta. Materialia.*, 2014, **79**, 30-36.
36 C. F. Vardeman and J. D. Gezelter, *J. Phys. Chem. C*, 2008, **112**, 3283-3293.
37 G. J. Li, X. P. Song, Z. B. Sun, S. C. Yang, B. J. Ding, S. Yang, Z. M. Yang and F. Wang, *Solid. State. Sci.*, 2011, **13**, 1379-1384.
38 Y. Lei, F. Chen, B. Huang and Z. Liu, *Mater. Res. Express*, 2014, **1**, 015031.
39 Y. L. Mikhlin, E. A. Vishnyakova, A. S. Romanchenko, S. V. Saikova, M. N. Likhatski, Y. V. Larichev, F. V. Tuzikov, V. I. Zaikovskii and S. M. Zharkov, *Appl. Sur. Sci.*, 2014, **297**, 75-83.
40 J. Banhart, H. Ebert, R. Kuentzler and J. Voitlander, *Phys. Rev. B*, 1992, **46**, 9968-9975.
41 J. Wang and S. Q. Wang, *Surf. Sci.*, 2014, **630**, 216-224.
42 M. F. Juarez and E. Santos, *J. Phys. Chem. C*, 2013, **117**, 4606-4618.
43 J. W. Niemantsverdriet, *Spectroscopy in catalysis* Wiley-VCH ; John Wiley, distributor, Weinheim Chichester, 2007.
44 K. Shin, D. H. Kim, S. C. Yeo and H. M. Lee, *Catal. Today*, 2012, **185**, 94-98.
45 T. H. Yang, S. Venkatesan, C. H. Lien, J. L. Chang and J. M. Zen, *Electrochim. Acta*, 2011, **56**, 6205-6210.
46 G. Du, X. Liu, Y. Zong, T. S. Hor, A. Yu and Z. Liu, *Nanoscale*, 2013, **5**, 4657-4661.
47 J. T. Zhang, Z. H. Zhao, Z. H. Xia and L. M. Dai, *Nat. Nanotechnol.*, 2015, **10**, 444-452.
48 J. S. Lee, G. S. Park, H. I. Lee, S. T. Kim, R. G. Cao, M. L. Liu and J. Cho, *Nano Lett.*, 2011, **11**, 5362-5366.
49 Z. Chen, J. Y. Choi, H. J. Wang, H. Li and Z. W. Chen, *J. Power Sources*, 2011, **196**, 3673-3677.
50 G. Doubek, R. C. Sekol, J. Li, W. H. Ryu, F. S. Gittleson, S. Nejati, E. Moy, C. Reid, M. Carmo, M. Linardi, P. Bordeenithikasem, E. Kinser, Y. Liu, X. Tong, C. O. Osuji, J. Schroers, S. Mukherjee and A.D. Taylor, *Adv. Mater.,* 2015, DOI: 10.1002/ adma.201504504.

The table of contents

A Silver-copper metallic glass (AgCu-MG) electrocatalyst has been fabricated for a rechargeable zinc-air battery by a pulsed laser deposition. The AgCu-MG exceptionally enhance their ORR catalytic activity after 1000 CV cycle treatment in 0.1 M KOH with a half-wave potential of 0.78V vs. RHE. The AgCu-MGs exhibit a high discharge voltage above 1.0 V at 20 mA cm^{-2} after discharged-charged for more than 1000 cycles when only air was used for test.

Xiaoqiang Wu,[a] Fuyi Chen, [a *] Nan Zhang,[a] Adnan Qaseem [a] and Roy L. Johnston [b *]

Title Silver-Copper Metallic Glass Electrocatalyst with High Activity and Stability Comparable to Pt/C for Zinc–Air Batteries

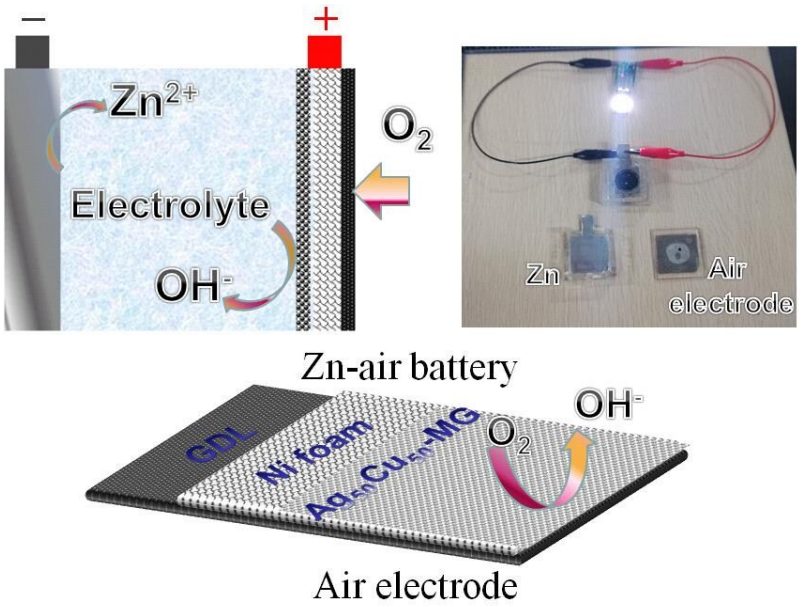

TOC Figure